

1 Creating and controlling visual environments 2 using BonVision

3

4 Gonçalo Lopes¹, Karolina Farrell^{2,‡}, Edward A. B. Horrocks^{2,‡}, Chi-Yu Lee^{2,‡}, Mai M. Morimoto^{2,‡},
5 Tomaso Muzzu^{2,‡}, Amalia Papanikolaou^{2,‡}, Fabio R. Rodrigues^{2,‡}, Thomas Wheatcroft^{2,‡}, Stefano
6 Zucca^{2,‡}, Samuel G. Solomon^{2,*}, Aman B. Saleem^{2,*}

7

8 ¹NeuroGEARS Ltd., London; ²UCL Institute of Behavioural Neuroscience, Department of Experimental Psychology,
9 University College London, London, WC1H 0AP.

10 [‡]These authors are listed alphabetically.

11 ^{*}These authors jointly supervised this work.

12 Lead Contact: Aman B Saleem (aman.saleem@ucl.ac.uk)

13

14 **Real-time rendering of closed-loop visual environments is important for next-generation**
15 **understanding of brain function and behaviour, but is often prohibitively difficult for non-experts**
16 **to implement and is limited to few laboratories worldwide. We developed BonVision as an easy-to-**
17 **use open-source software for the display of virtual or augmented reality, as well as standard visual**
18 **stimuli. BonVision has been tested on humans and mice, and is capable of supporting new**
19 **experimental designs in other animal models of vision. As the architecture is based on the open-**
20 **source Bonsai graphical programming language, BonVision benefits from native integration with**
21 **experimental hardware. BonVision therefore enables easy implementation of closed-loop**
22 **experiments, including real-time interaction with deep neural networks, and communication with**
23 **behavioural and physiological measurement and manipulation devices.**

24

25 Introduction

26 Understanding behaviour and its underlying neural mechanisms calls for the ability to construct
27 and control environments that immerse animals, including humans, in complex naturalistic
28 environments that are responsive to their actions. Gaming-driven advances in computation and
29 rendering have driven the development of immersive closed-loop visual environments, but
30 these new platforms are not readily amenable to traditional research paradigms. For example,
31 they do not specify an image in egocentric units (of visual angle), sacrifice precise control of a
32 visual display, and lack transparent interaction with external hardware.

33 Most vision research has been performed in non-immersive environments with standard two-
34 dimensional visual stimuli, such as gratings or dot stimuli, using established platforms including
35 PsychToolbox¹ or PsychoPy^{2,3}. Pioneering efforts to bring gaming-driven advances to
36 neuroscience research have provided new platforms for closed-loop visual stimulus generation:
37 STYTRA⁴ provides 2D visual stimuli for larval zebrafish in python, ratCAVE⁵ is a specialised
38 augmented reality system for rodents in python, FreemoVR⁶ provides virtual reality in
39 Ubuntu/Linux, and ViRMEn⁷ provides virtual reality in Matlab. However, these new platforms
40 lack the generalised frameworks needed to specify or present standard visual stimuli.

41 Our initial motivation was to create a visual display software with three key features. First, an
42 integrated, standardised platform that could rapidly switch between traditional visual stimuli
43 (such as grating patterns) and immersive virtual reality. Second, the ability to replicate
44 experimental workflows across different physical configurations (for example, when moving

45 from one to two computer monitors, or from flat-screen to spherical projection). Third, the
46 ability for rapid and efficient interfacing with external hardware (needed for experimentation)
47 without development of complex multi-threaded routines. We wanted to provide these
48 advances in a way that made it easier for users to construct and run closed-loop experimental
49 designs. In closed-loop experiments stimuli are ideally conditioned by asynchronous inputs,
50 such as those provided by multiple independent behavioural and neurophysiological
51 measurement devices. Most existing platforms require the development of multi-threaded
52 routines to run experimental paradigms (e.g. control brain stimulation, or sample from
53 recording devices) without compromising the rendering of visual scenes. Implementing such
54 multi-thread routines is complex. We therefore chose to develop a visual presentation
55 framework within the Bonsai programming language⁸. Bonsai is a graphical, high-performance,
56 and event-based language that is widely used in neuroscience experiments and is already
57 capable of real-time interfacing with most types of external hardware. Bonsai is specifically
58 designed for flexible and high-performance composition of data streams and external events,
59 and is therefore able to monitor and connect multiple sensor and effector systems in parallel,
60 making it easier to implement closed-loop experimental designs.

61
62 We developed BonVision, an open-source software package that can generate and display well-
63 defined visual stimuli in 2D and 3D environments. BonVision exploits Bonsai's ability to run
64 OpenGL commands on the graphics card through the Bonsai.Shaders package. BonVision
65 further extends Bonsai by providing pre-built GPU shaders and resources for stimuli used in
66 vision research, including movies, along with an accessible, modular interface for composing
67 stimuli and designing experiments. The definition of stimuli in BonVision is independent of the
68 display hardware, allowing for easy replication of workflows across different experimental
69 configurations. Additional unique features include the ability to automatically detect and define
70 the relationship between the observer and the display from a photograph of the experimental
71 apparatus, and to use the outputs of real-time inference methods to determine the position
72 and pose of an observer online, thereby generating augmented reality environments.

73
74 **Results**
75 To provide a framework that allowed both traditional visual presentation and immersive virtual
76 reality, we needed to bring these very different ways of defining the visual scene into the same
77 architecture. We achieved this by mapping the 2D retino-centric coordinate frame (i.e. degrees
78 of the visual field) to the surface of a 3D sphere using the Mercator projection (Fig 1A, Suppl.
79 Fig 1). The resulting sphere could therefore be rendered onto displays in the same way as any
80 other 3D environment. We then used "cube mapping" to specify the 360° projection of 3D
81 environments onto arbitrary viewpoints around an experimental observer (human or animal;
82 Fig 1B). Using this process, a display device becomes a window into the virtual environment,
83 where each pixel on the display specifies a vector from the observer through that window. The
84 vector links pixels on the display to pixels in the 'cube map', thereby rendering the
85 corresponding portion of the visual field onto the display.

86
87 Our approach has the advantage that the visual stimulus is defined irrespectively of display
88 hardware, allowing us to independently define each experimental apparatus without changing
89 the preceding specification of the visual scene, or the experimental design (Fig 1C-E, Suppl. Fig
90 1, 2). Consequently, BonVision makes it easy to replicate visual environments and experimental
91 designs on various display devices, including multiple monitors, curved projection surfaces, and

92 head-mounted displays (Fig 1C-E). To facilitate easy and rapid porting between different
93 experimental apparatus, BonVision features a fast semi-automated display calibration. A
94 photograph of the experimental setup with fiducial markers⁹ measures the 3D position and
95 orientation of each display relative to the observer (Fig 2 and Fig 2 – figure supplement 1).
96 BonVision’s inbuilt image processing algorithms then estimate the position and orientation of
97 each marker to fully specify the display environment.

98 Virtual reality environments are easy to generate in BonVision. BonVision has a library of
99 standard pre-defined 3D structures (including planes, spheres and cubes), and environments
100 can be defined by specifying the position and scale of the structures, and the textures rendered
101 on them (e.g. Figure 1 – figure supplement 2 and Fig. 5F). BonVision also has the ability to
102 import standard format 3D design files created elsewhere in order to generate more complex
103 environments (file formats listed in Methods). This allows users to leverage existing 3D drawing
104 platforms (including open source platform ‘Blender’: <https://www.blender.org/>) to construct
105 complex virtual scenes (see Appendix).

106 BonVision can define the relationship between the display and the observer in real-time. This
107 makes it easy to generate augmented reality environments, where what is rendered on a
108 display depends on the position of an observer (Fig 3A). For example, when a mouse navigates
109 through an arena surrounded by displays, BonVision enables closed-loop, position-dependent
110 updating of those displays. Bonsai can track markers to determine the position of the observer,
111 but it also has turn-key capacity for real-time live pose estimation techniques – using deep
112 neural networks^{10,11} – to keep track of the observer’s movements. This allows users to generate
113 and present interactive visual environments (simulation in Fig 3 - video 1 and Fig 3B-C).

114 BonVision is capable of rendering visual environments near the limits of the hardware (Fig 4).
115 This is possible because Bonsai is based on a just-in-time compiler architecture such that there
116 is little computational overhead. BonVision accumulates a list of the commands to OpenGL as
117 the program makes them. To optimise rendering performance, the priority of these commands
118 is ordered according to that defined in the Shaders component of the *LoadResources* node
119 (which the user can manipulate for high-performance environments). These ordered calls are
120 then executed when the frame is rendered. To benchmark the responsiveness of BonVision in
121 closed-loop experiments, we measured the delay (latency) between an external event and the
122 presentation of a visual stimulus. We first measured the closed-loop latency for BonVision
123 when a monitor was refreshed at a rate of 60Hz (Fig 4A). We found delays averaged 2.11 ± 0.78
124 frames (35.26 ± 13.07 ms). This latency was slightly shorter than that achieved by
125 PsychToolbox¹³ on the same laptop (2.44 ± 0.59 frames, 40.73 ± 9.8 ms; Welch’s t-test, $p < 10^{-80}$,
126 $n=1000$). The overall latency of BonVision was mainly constrained by the refresh rate of the
127 display device, such that higher frame rate displays yielded lower latency (60Hz: $35.26 \pm$
128 13.07 ms; 90Hz: 28.45 ± 7.22 ms; 144Hz: 18.49 ± 10.1 ms; Fig 4A). That is, the number of frames
129 between the external event and stimulus presentation was fairly constant across frame rate
130 (60Hz: 2.11 ± 0.78 frames; 90Hz: 2.56 ± 0.65 frames; 144Hz: 2.66 ± 1.45 frames; Fig 4C). We
131 used two additional methods to benchmark visual display performance relative to other
132 frameworks (we did not try to optimise code fragments for each framework) (Fig 4B-C).
133 BonVision was able to render up to 576 independent elements and up to 8 overlapping
134 textures at 60Hz without missing (‘dropping’) frames, broadly matching PsychoPy^{2,3} and
135 Psychtoolbox¹. BonVision’s performance was similar at different frame rates - at standard

136 frame rate (60 Hz), and at 144Hz (Figure 4 - figure supplement 1). BonVision could achieve
137 slightly fewer overlapping textures than PsychoPy, as BonVision does not currently have the
138 option to trade-off the resolution of a texture and its mask for performance. BonVision also
139 supports video playback, either by preloading the video or by streaming it from the disk. The
140 streaming mode, which utilises real-time file I/O and decompression, is capable of displaying
141 both standard definition (SD: 480p) and full HD (HD: 1080p) at 60Hz on a standard computer
142 (Fig 4D). At higher rates, performance is impaired for Full HD videos, but is improved by
143 buffering, and fully restored by preloading the video onto memory (Fig 4D). We benchmarked
144 BonVision on a standard Windows OS laptop, but BonVision is now also capable of running on
145 Linux.

146 To confirm that the rendering speed and timing accuracy of BonVision is sufficient to support
147 neurophysiological experiments, which need high timing accuracy, we mapped the receptive
148 fields of neurons early in the visual pathway¹², in the mouse primary visual cortex and superior
149 colliculus. The stimulus ('sparse noise') consisted of small black or white squares briefly (0.1s)
150 presented at random locations (Fig 5A). This stimulus, which is commonly used to measure
151 receptive fields of visual neurons, is sensitive to the timing accuracy of the visual stimulus,
152 meaning that errors in timing would prevent the identification of receptive fields. In our
153 experiments using BonVision, we were able to recover receptive fields from
154 electrophysiological measurements¹³ - both in the superior colliculus and primary visual cortex
155 of awake mice (Fig 5B-C) - demonstrating that BonVision meets the timing requirements for
156 visual neurophysiology. The receptive fields show in Fig 5C were generated using timing signals
157 obtained directly from the stimulus display (via a photodiode). BonVision's independent logging
158 of stimulus presentation timing was also sufficient to capture the receptive field (Fig 5 - figure
159 supplement 1).

160 To assess the ability of BonVision to control virtual reality environments we first tested its
161 ability to present stimuli to human observers on a head-mounted display¹⁴. BonVision uses
162 positional information (obtained from the head-mounted display) to update the view of the
163 world that needs to be provided to each eye, and returns two appropriately rendered images.
164 On each trial, we asked observers to identify the larger of two non-overlapping cubes that were
165 placed at different virtual depths (Fig 5D-E). The display was updated in closed-loop to allow
166 observers to alter their viewpoint by moving their head. Distinguishing objects of the same
167 retinal size required observers to use depth-dependent cues¹⁵, and we found that all observers
168 were able to identify which cube was larger (Fig 5E).

169 We next asked if BonVision was capable of supporting other visual display environments that
170 are increasingly common in the study of animal behaviour. We first projected a simple
171 environment onto a dome that surrounded a head-fixed mouse (as shown in Fig 1E). The
172 mouse was free to run on a treadmill, and the treadmill's movements were used to update the
173 mouse's position on a virtual platform (Fig 5F). Not only did mouse locomotion speed increase
174 with repeated exposure, but the animals modulated their speed depending on their location in
175 the platform (Fig 5F-G). BonVision is therefore capable of generating virtual reality
176 environments which both elicit, and are responsive to animal behaviour. BonVision was also
177 able to produce instinctive avoidance behaviours in freely-moving mice (Fig 5H-I). We displayed
178 a small black dot slowly sweeping across the overhead visual field. Visual stimuli presented in
179 BonVision primarily elicited a freezing response, which similar experiments have previously

180 described¹⁰ (Fig 5I). Together these results show that BonVision provides sufficient rendering
181 performance to support human and animal visual behaviour.

182 Discussion

183 BonVision is a single software package to support experimental designs that require visual
184 display, including virtual and augmented reality environments. BonVision is easy and fast to
185 implement, cross-platform and open source, providing versatility and reproducibility.

186 BonVision makes it easier to address several barriers to reproducibility in visual experiments.
187 First, BonVision is able to replicate and deliver visual stimuli on very different experimental
188 apparatus. This is possible because BonVision's architecture separates specification of the
189 display and the visual environment. Second, BonVision includes a library of workflows and
190 operators to standardize and ease the construction of new stimuli and virtual environments.
191 For example, it has established protocols for defining display positions (Suppl. Fig 3), mesh-
192 mapping of curved displays (Fig 1E), and automatic linearization of display luminance (Suppl.
193 Fig 4), as well as a library of examples for experiments commonly used in visual neuroscience.
194 In addition, the modular structure of BonVision enables the development and exchange of
195 custom nodes for generating new visual stimuli or functionality without the need to construct
196 the complete experimental paradigm. Third, BonVision is based on Bonsai⁸, which has a large
197 user base and an active developer community, and is now a standard tool for open-source
198 neuroscience research. BonVision naturally integrates Bonsai's established packages in the
199 multiple domains important for modern neuroscience, which are widely used in applications
200 including real-time video processing^{16,17}, optogenetics¹⁶⁻¹⁸, fibre photometry^{19,20},
201 electrophysiology (including specific packages for Open Ephys^{13,21} and high-density silicon
202 probes^{22,23}), and calcium imaging (e.g. UCLA miniscope^{24,25}). Bonsai requires researchers to get
203 accustomed to its graphical interface and event-based framework. However, it subsequently
204 reduces the time required to learn real-time programming, and the time to build new
205 interfaces with external devices (see Appendix). Moreover, since Bonsai workflows can be
206 called via the command line, BonVision can also be integrated into pre-existing, specialised
207 frameworks in established laboratories.

208 In summary, BonVision can generate complex 3D environments and retinotopically defined 2D
209 visual stimuli within the same framework. Existing platforms used for vision research, including
210 PsychToolbox¹, PsychoPy^{2,3}, STYTRA⁷, or RigBox²⁶, focus on well-defined 2D stimuli. Similarly,
211 gaming-driven software, including FreemoVR⁴, ratCAVE⁵, and ViRMEn⁶, are oriented towards
212 generating virtual reality environments. BonVision combines the advantages of both these
213 approaches in a single framework (Supplementary file 1), while bringing the unique capacity to
214 automatically calibrate the display environment, and use deep neural networks to provide real-
215 time control of virtual environments. Experiments in BonVision can be rapidly prototyped and
216 easily replicated across different display configurations. Being free, open-source and portable,
217 BonVision is a state-of-the-art tool for visual display that is accessible to the wider community.

218 Code availability

219 BonVision is an open-source software package available to use under the MIT license. It can be
220 downloaded through the Bonsai (bonsai-rx.org) package manager, and the source code is
221 available at: github.com/bonvision/BonVision. All benchmark programs and data are available

222 at <https://github.com/bonvision/benchmarks>. Installation instructions, demos and learning
223 tools are available at: bonvision.github.io/.

224 Acknowledgements

225 We are profoundly thankful to Bruno Cruz and Joe Paton for sharing their videos of mouse
226 behaviour. This work was supported by a Wellcome Enrichment award: Open Research
227 (200501/Z/16/A), Sir Henry Dale Fellowship from the Wellcome Trust and Royal Society
228 (200501), Human Science Frontiers Program grant (RGY0076/2018) to A.B.S., an International
229 Collaboration Award (with Adam Kohn) from the Stavros Niarchos Foundation / Research to
230 Prevent Blindness to S.G.S., Medical Research Council grant (R023808), Biotechnology and
231 Biological Sciences Research Council grant (R004765) to S.G.S. and A.B.S.

232 Author Contributions

233 This work was conceptualised by G.L., S.G.S. and A.B.S., the software was developed by G.L.,
234 methodology and validation were by all authors, writing – original draft was by G.L., S.G.S. and
235 A.B.S., and writing – review & editing was by G.L., K.F., M.M.M., T.M., F.R.R., T.W., S.Z., S.G.S. &
236 A.B.S, and supervision and funding acquisition was by S.G.S. and A.B.S.

237

238 References

- 239 1. Brainard, D. H. The Psychophysics Toolbox. *Spat. Vis.* **10**, 433–436 (1997).
- 240 2. Peirce, J. W. PsychoPy-Psychophysics software in Python. *J. Neurosci. Methods* **162**, 8–13
241 (2007).
- 242 3. Peirce, J. W. Generating stimuli for neuroscience using PsychoPy. *Front. Neuroinform.* **2**,
243 (2009).
- 244 4. Stowers, J. R. *et al.* Virtual reality for freely moving animals. *Nat. Methods* **14**, 995–1002
245 (2017).
- 246 5. Del Grosso, N. A. & Sirota, A. Ratcave: A 3D graphics python package for cognitive
247 psychology experiments. *Behav. Res. Methods* **51**, 2085–2093 (2019).
- 248 6. Aronov, D. & Tank, D. W. Engagement of Neural Circuits Underlying 2D Spatial
249 Navigation in a Rodent Virtual Reality System. *Neuron* **84**, 442–456 (2014).
- 250 7. Štih, V., Petrucco, L., Kist, A. M. & Portugues, R. Stytra: An open-source, integrated
251 system for stimulation, tracking and closed-loop behavioral experiments. *PLOS Comput.*
252 *Biol.* **15**, e1006699 (2019).
- 253 8. Lopes, G. *et al.* Bonsai: an event-based framework for processing and controlling data
254 streams. *Front. Neuroinform.* **9**, 7 (2015).
- 255 9. Garrido-Jurado, S., Muñoz-Salinas, R., Madrid-Cuevas, F. J. & Marín-Jiménez, M. J.
256 Automatic generation and detection of highly reliable fiducial markers under occlusion.
257 *Pattern Recognit.* **47**, 2280–2292 (2014).
- 258 10. Mathis, A. *et al.* DeepLabCut: markerless pose estimation of user-defined body parts
259 with deep learning. *Nat. Neurosci.* **21**, 1281–1289 (2018).
- 260 11. Pereira, T. D. *et al.* Fast animal pose estimation using deep neural networks. *Nat.*
261 *Methods* **16**, 117–125 (2019).
- 262 12. Yeh, C. I., Xing, D., Williams, P. E. & Shapley, R. M. Stimulus ensemble and cortical layer
263 determine V1 spatial receptive fields. *Proc. Natl. Acad. Sci. U. S. A.* **106**, 14652–14657
264 (2009).
- 265 13. Siegle, J. H. *et al.* Open Ephys: An open-source, plugin-based platform for multichannel

266 electrophysiology. *J. Neural Eng.* **14**, 045003 (2017).

267 14. Scarfe, P. & Glennerster, A. Using high-fidelity virtual reality to study perception in freely
268 moving observers. *J. Vis.* **15**, 3–3 (2015).

269 15. Rolland, J. P., Gibson, W. & Ariely, D. Towards Quantifying Depth and Size Perception in
270 Virtual Environments. *Presence Teleoperators Virtual Environ.* **4**, 24–49 (1995).

271 16. Zacarias, R., Namiki, S., Card, G. M., Vasconcelos, M. L. & Moita, M. A. Speed dependent
272 descending control of freezing behavior in *Drosophila melanogaster*. *Nat. Commun.* **9**, 1–
273 11 (2018).

274 17. Buccino, A. P. *et al.* Open source modules for tracking animal behavior and closed-loop
275 stimulation based on Open Ephys and Bonsai. *J. Neural Eng.* **15**, (2018).

276 18. Moreira, J. M. *et al.* Optopad, a closed-loop optogenetics system to study the circuit
277 basis of feeding behaviors. *Elife* **8**, (2019).

278 19. Soares, S., Atallah, B. V. & Paton, J. J. Midbrain dopamine neurons control judgment of
279 time. *Science (80-.)*. **354**, 1273–1277 (2016).

280 20. Hrvatin, S. *et al.* Neurons that regulate mouse torpor. *Nature* 1–7 (2020).
281 doi:10.1038/s41586-020-2387-5

282 21. Neto, J. P. *et al.* Validating silicon polytrodes with paired juxtacellular recordings:
283 Method and dataset. *J. Neurophysiol.* **116**, 892–903 (2016).

284 22. Jun, J. J. *et al.* Fully integrated silicon probes for high-density recording of neural activity.
285 *Nature* **551**, 232–236 (2017).

286 23. Dimitriadis, G. *et al.* Why not record from every channel with a CMOS scanning probe?
287 *bioRxiv* 275818 (2018). doi:10.1101/275818

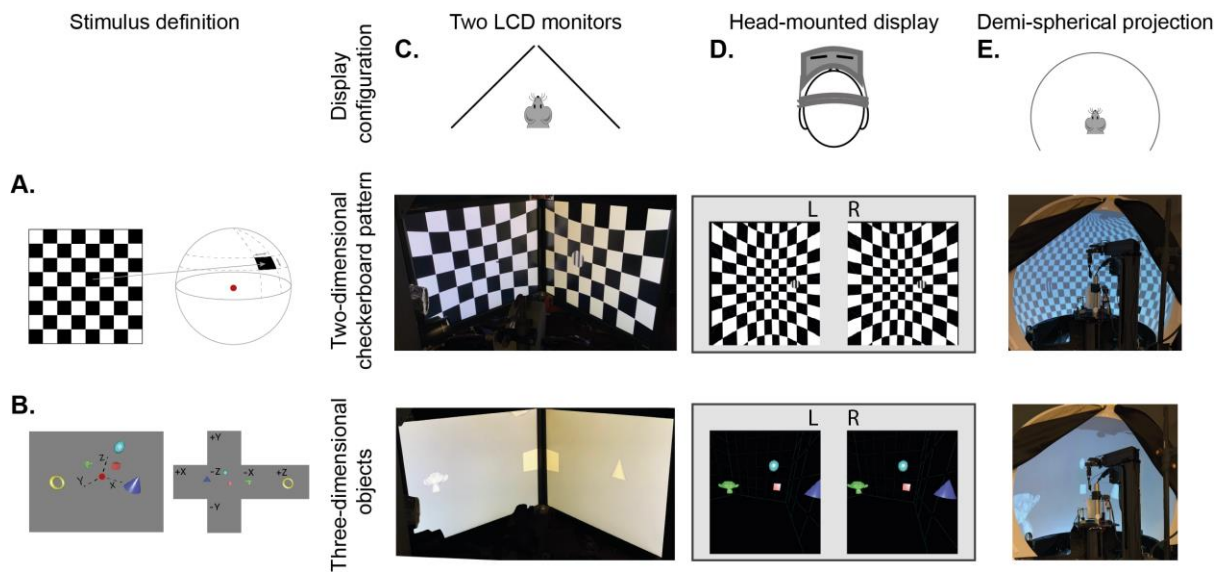
288 24. Aharoni, D., Khakh, B. S., Silva, A. J. & Golshani, P. All the light that we can see: a new era
289 in miniaturized microscopy. *Nature Methods* **16**, 11–13 (2019).

290 25. Cai, D. J. *et al.* A shared neural ensemble links distinct contextual memories encoded
291 close in time. *Nature* **534**, 115–118 (2016).

292 26. Bhagat, J., Wells, M. J., Harris, K. D., Carandini, M. & Burgess, C. P. Rigbox: An Open-
293 Source Toolbox for Probing Neurons and Behavior. *eneuro* ENEURO.0406-19.2020
294 (2020). doi:10.1523/ENEURO.0406-19.202

295 **Figures**

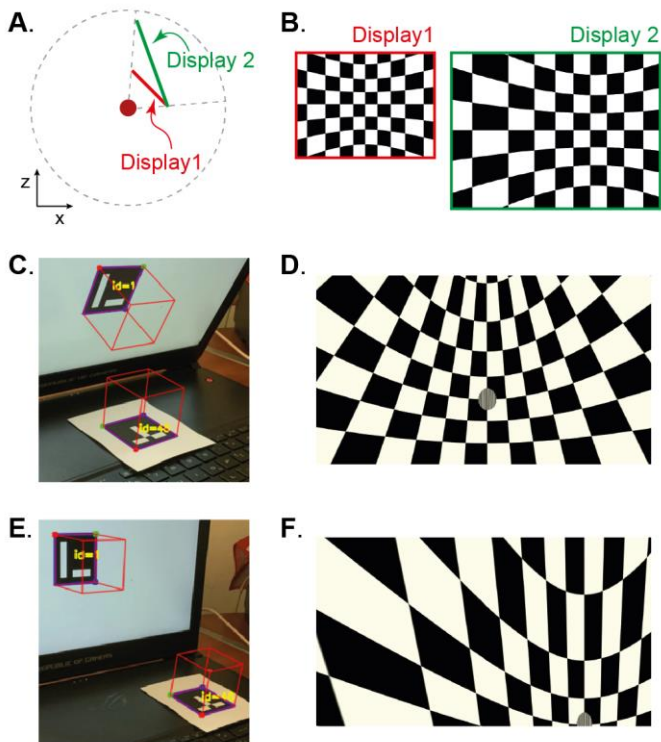
296



297

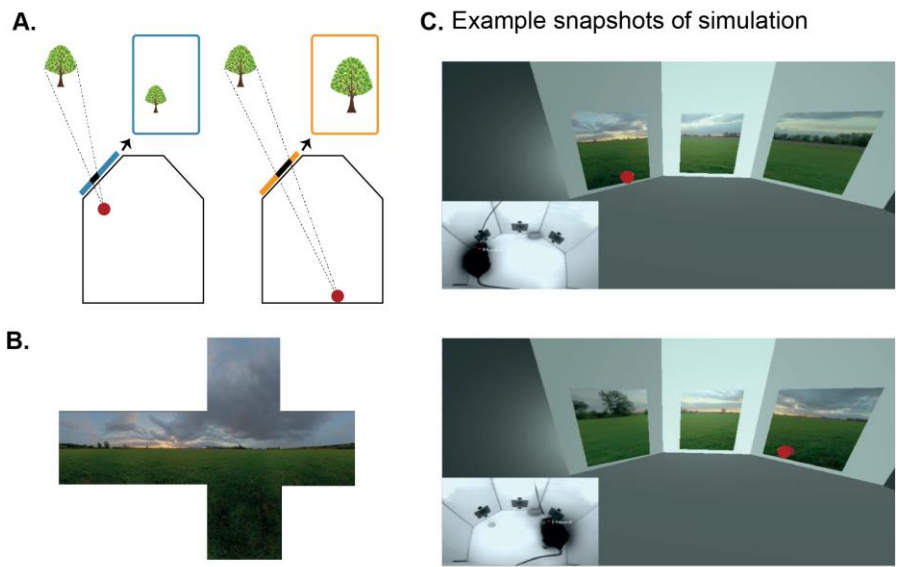
298 **Figure 1: BonVision adaptable display and render configurations.** A. Illustration of how
 299 two-dimensional textures are generated in BonVision using Mercator projection for sphere
 300 mapping, with elevation as latitude and azimuth as longitude. The red dot indicates the
 301 position of the observer. B. Three-dimensional objects were placed at the appropriate
 302 positions and the visual environment was rendered using cube-mapping. C-E. Examples of
 303 the same two stimuli, a checkerboard + grating (middle row) or four three-dimensional
 304 objects (bottom row), displayed in different experimental configurations (top row): two
 305 angled LCD monitors (C), a head-mounted display (D), and demi-spherical dome (E).

306



308

309 **Figure 2: Automated calibration of display position.** **A.** Schematic showing the position of
 310 two hypothetical displays of different sizes, at different distances and orientation relative
 311 to the observer (red dot). **B.** How a checkerboard of the same visual angle would appear on
 312 each of the two displays. **C.** Example of automatic calibration of display position. Standard
 313 markers are presented on the display, or in the environment, to allow automated detection
 314 of the position and orientation of both the display and the observer. These positions and
 315 orientations are indicated by the superimposed red cubes as calculated by BonVision. **D.**
 316 How the checkerboard would appear on the display when rendered, taking into account the
 317 precise position of the display. **E-F.** Same as **C-D**, but for another pair of display and
 318 observer positions. The automated calibration was based on the images shown in **C** and **E**.

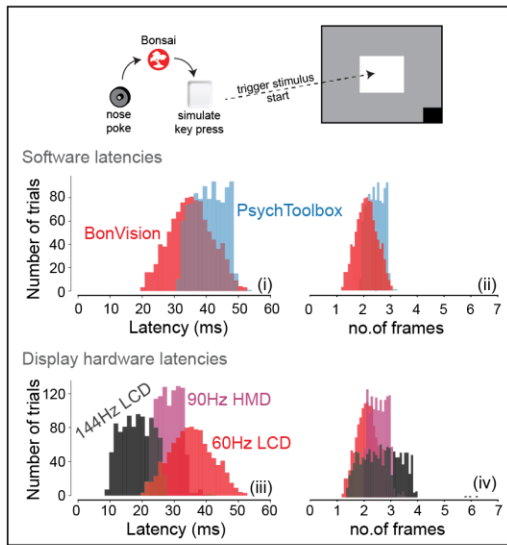


319

320 **Figure 3: Using BonVision to generate an augmented reality environment.** **A.** Illustration of
 321 how the image on a fixed display needs to adapt as an observer (red dot) moves around an
 322 environment. The displays simulate windows from a box into a virtual world outside. **B.** The
 323 virtual scene (from: <http://scmapdb.com/wad:skybox-skies>) that was used to generate the
 324 example images and Figure 3 - Video 1 offline. **C.** Real-time simulation of scene rendering in
 325 augmented reality. We show two snapshots of the simulated scene rendering, which is also
 326 shown in Figure 3 - video 1. In each case the inset image shows the actual video images, of a
 327 mouse exploring an arena, that were used to determine the viewpoint of an observer in the
 328 simulation. The mouse's head position was inferred (at a rate of 40 frames/s) by a network
 329 trained using DeepLabCut⁶. The top image shows an instance when the animal was on the
 330 left of the arena (head position indicated by the red dot in the main panel) and the lower
 331 image shows an instance when it was on the right of the arena.

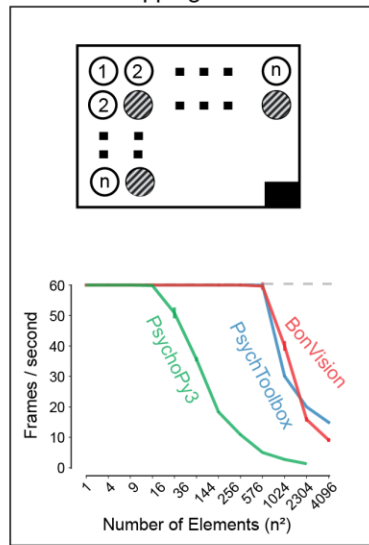
332

A. Closed-loop latency tests



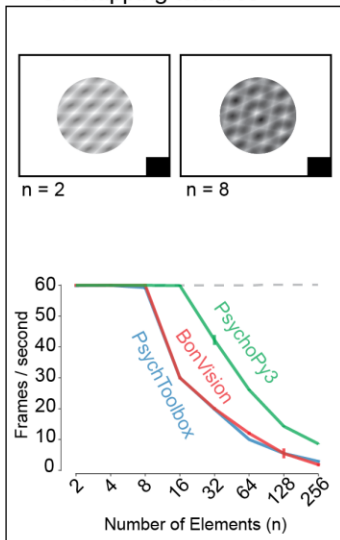
B. Stress tests

Non-overlapping textures



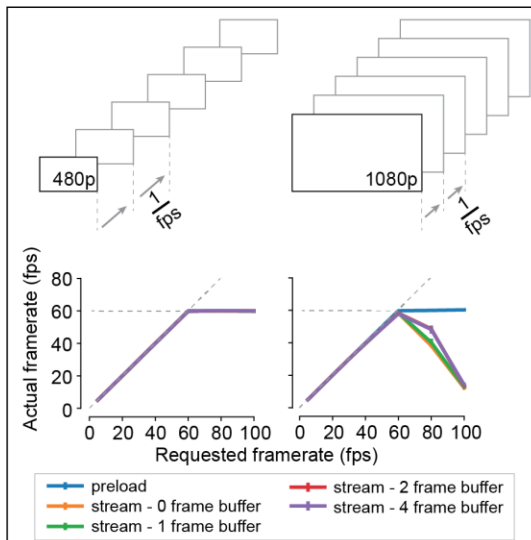
C. Stress tests

Overlapping textures



D. Stress tests

Video Resolution



333

334

335

336

337

338

339

340

341

342

343

344

345

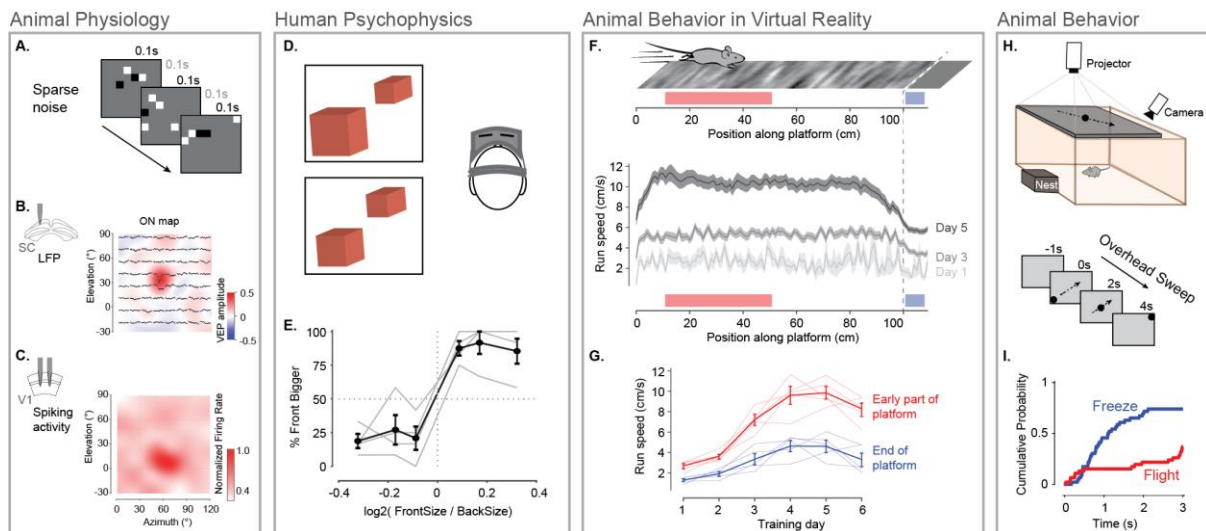
346

347

Figure 4: Closed-loop latency and performance benchmarks. **A.** Latency between sending a command (virtual key press) and updating the display (measured using a photodiode). (A.i - A.ii) Latency depended on the frame rate of the display, updating stimuli with a delay of 1-3 frames. (A.iii - A.iv). **B-C.** Benchmarked performance of BonVision with respect to Psychtoolbox and PsychoPy. **B.** When using non-overlapping textures BonVision and Psychtoolbox could present 576 independent textures without dropping frames, while PsychoPy could present 16. **C.** When using overlapping textures PsychoPy could present 16 textures, while BonVision and Psychtoolbox could present 8 textures without dropping frames. **D.** Benchmarks for movie playback. BonVision is capable of displaying standard definition (480p) and high definition (1080p) movies at 60 frames/s on a laptop computer with a standard CPU and graphics card. We measured display rate when fully pre-loading the movie into memory (blue), or when streaming from disk (with no buffer: orange; 1-frame buffer: green; 2-frame buffer: red; 4-frame buffer: purple). When asked to display at rates higher than the monitor refresh rate (>60 frames/s), the 480p video played at the

348 maximum frame rate of 60fps in all conditions, while the 1080p video reached the
 349 maximum rate when pre-loaded. Using a buffer slightly improved performance. A black
 350 square at the bottom right of the screen in A-C is the position of a flickering rectangle, which
 351 switches between black and white at every screen refresh. The luminance in this square is
 352 detected by a photodiode and used to measure the actual frame flip times.

353



354

355 **Figure 5: Illustration of BonVision across a range of vision research experiments.** **A.** Sparse
 356 noise stimulus, generated with BonVision, is rendered onto a demi-spherical screen. **B-C.**
 357 Receptive field maps from recordings of local field potential in the superior colliculus (**B**),
 358 and spiking activity in the primary visual cortex (**C**) of mouse. **D.** Two cubes were presented
 359 at different depths in a virtual environment through a head-mounted display to human
 360 subjects. Subjects had to report which cube was larger: left or right. **E.** Subjects
 361 predominantly reported the larger object correctly, with a slight bias to report that the
 362 object in front was bigger. **F.** BonVision was used to generate a closed-loop virtual platform
 363 that a mouse could explore (top: schematic of platform). Mice naturally tended to run faster
 364 along the platform, and in later sessions developed a speed profile, where they slowed
 365 down as they approached the end of the platform (virtual cliff). **G.** The speed of the animal
 366 at the start of the platform and at the end of the platform as a function training. **H.**
 367 BonVision was used to present visual stimuli overhead while an animal was free to explore
 368 an environment (which included a refuge). The stimulus was a small dot (5° diameter)
 369 moving across the projected surface over several seconds. **I.** The cumulative probability of
 370 Freeze and Flight behaviour across time in response to moving dot presented overhead.

371

372

373

374

375 **Supplementary file 1:** Features of visual display software✓✓ easy and well-supported

376

377

378

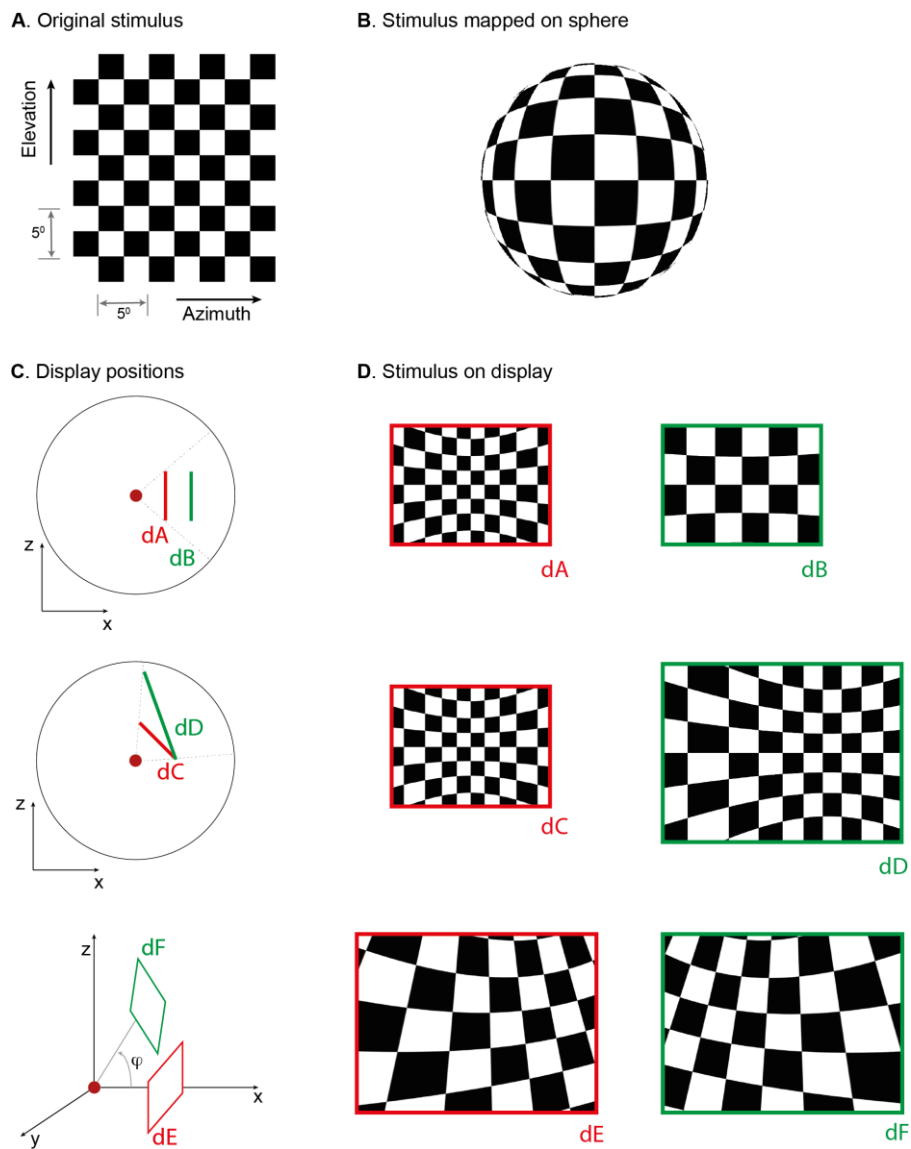
379

380

381

382 Supplementary Figures

383



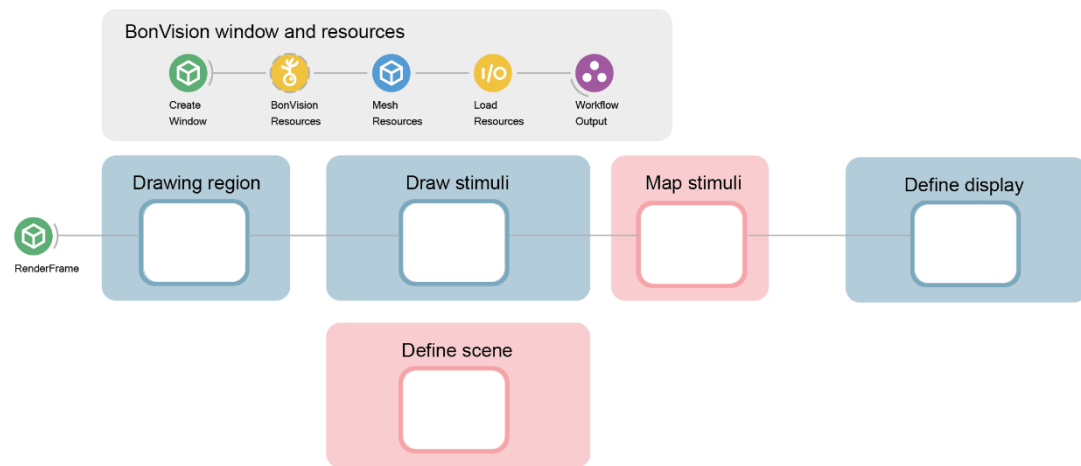
384

385 **Figure 1 - figure supplement 1: Mapping stimuli onto displays in various positions.**

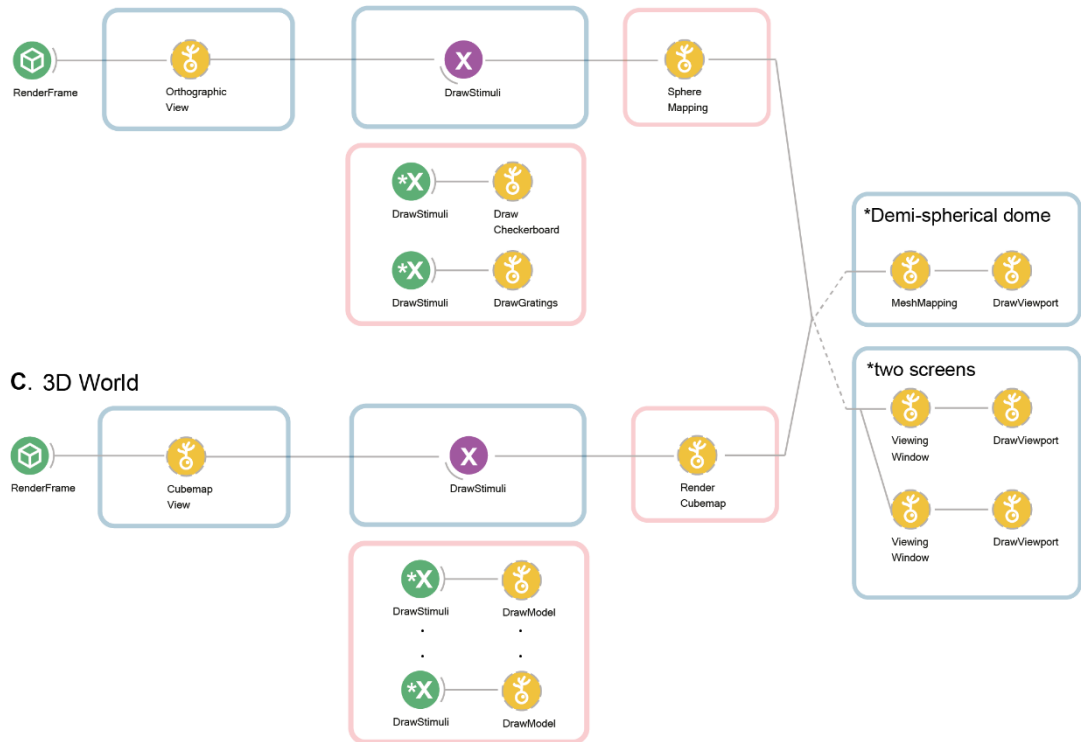
386 **A.** Checkerboard stimulus being rendered. **B.** Projection of the stimulus onto a sphere using
387 Mercator projection. **C.** Example display positions (dA-dF) and **(D)** corresponding rendered
388 images. Red dot in **C** indicates the observer position.

389

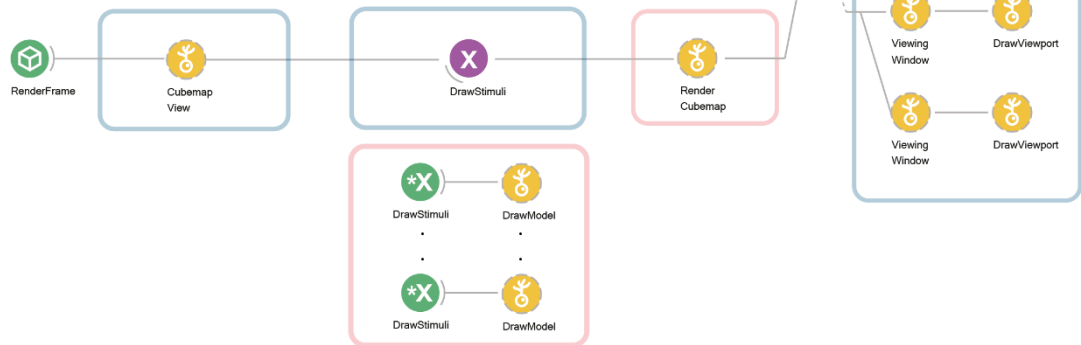
A. Modular structure of BonVision stimulus definition



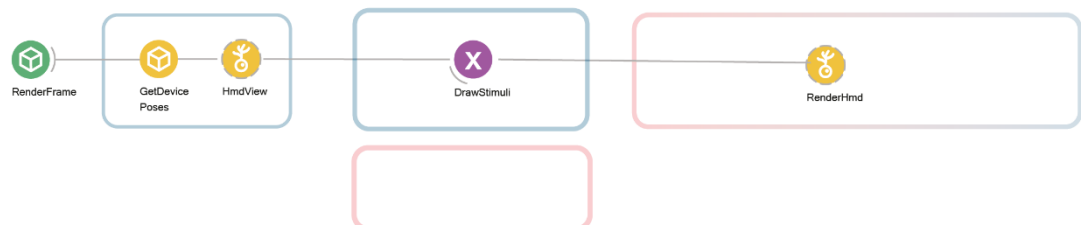
B. Checkerboard + Grating stimulus



C. 3D World



D. Stimuli on Head-mounted display (HMD)



390

391

Figure 1 - figure supplement 2: Modular structure of workflow and example workflows.

392

A. Description of the modules in BonVision workflows that generate stimuli. Every BonVision

393

stimuli includes a module that creates and initializes the render window, shown in

394

“BonVision window and resources”. This defines the window parameters in *Create Window*

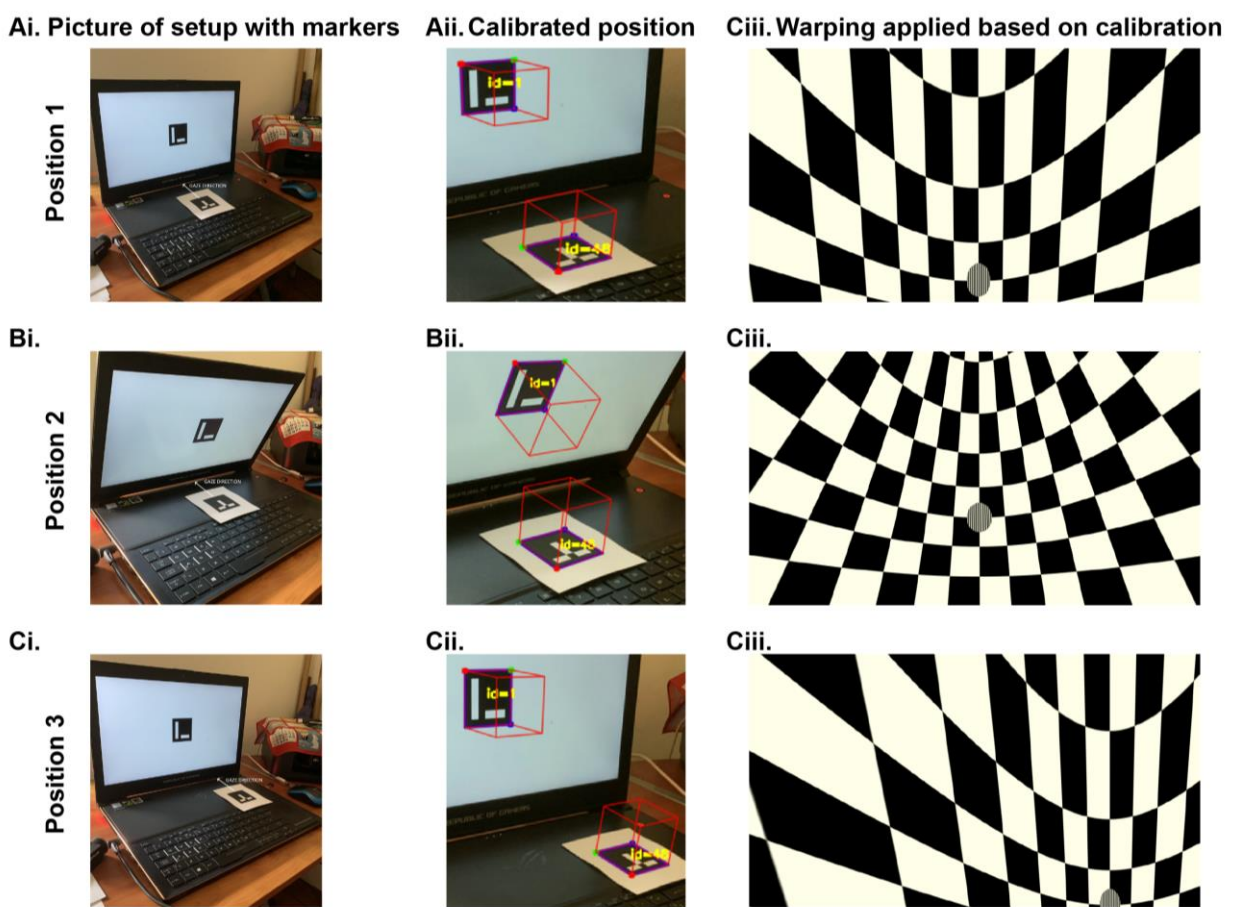
395

(such as background colour, screen index, VSync), and loads predefined (*BonVision*

396

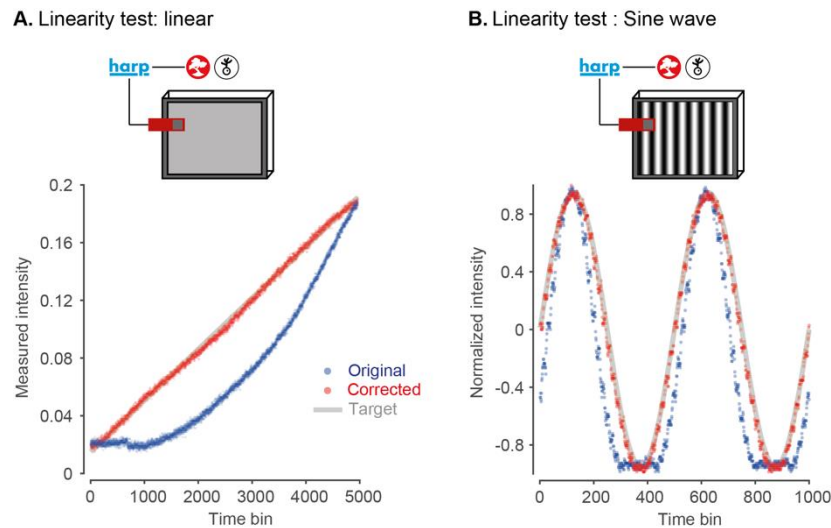
Resources) and user defined textures (*Texture Resources*, not shown), and 3D meshes (*Mesh*

397 Resources). This is followed by the modules: “Drawing region”, where the visual space
 398 covered by the stimuli is defined, which can be the complete visual space, 360° x 360°.
 399 “Draw stimuli” and “Define scene” are where the stimulus is defined, “Map Stimuli”, which
 400 maps the stimuli into the 3D environment, and “Define display”, where the display devices
 401 are defined. **B-C**. Modules that define the checkerboard + grating stimulus (**B**) shown in the
 402 middle row of Fig 1, and 3D world (**C**) with 5 objects shown in the bottom row of Fig 1. The
 403 display device is defined separately and either display can be appended at the end of the
 404 workflow. This separation of the display device allows for replication between experimental
 405 configurations. **D**. The variants of the modules used to display stimuli on a head-mounted
 406 display. The empty region under “Define scene” would be filled by the corresponding nodes
 407 in **B** and **C**.
 408
 409



410
 411 **Figure 2 - figure supplement 1: Automated workflow to calibrate display position.** The
 412 automated calibration is carried out by taking advantage of ArUco markers⁵ that can be
 413 used to calculate the 3D position of a surface. **Ai**. We use one marker on the display and one
 414 placed in the position of the observer. We then use a picture of the display and observer
 415 position taken by a calibrated camera. This is an example where we used a mobile phone
 416 camera for calibration. **Aii**. The detected 3D positions of the screen and the observer, as
 417 calculated by BonVision. **Aiii**. A checkerboard image and a small superimposed patch of
 418 grating, rendered based on the precise position of the display. **B-C**. same as A-C for different
 419 screen and observer positions: with the screen tilted towards the animal (**B**), or the observer

420 shifted to the right of the screen (C). The automated calibration was based on the images
421 shown in Ai, Bi and Ci, which in this case were taken using a mobile phone camera.
422
423
424

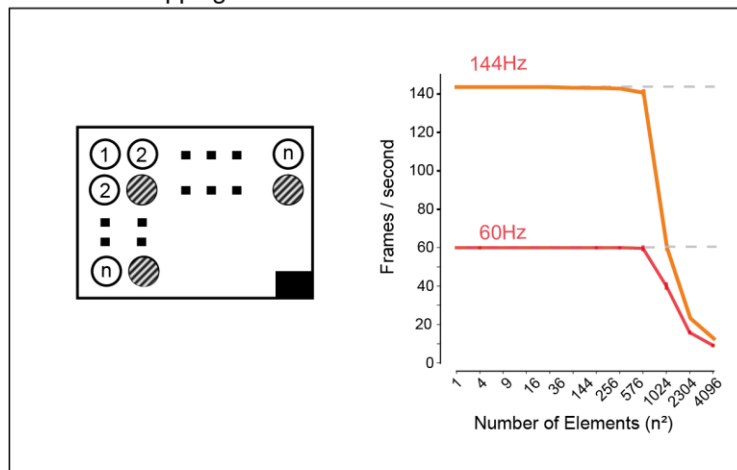


425
426
427 **Figure 2 - figure supplement 2: Automated gamma-calibration of visual displays.** BonVision
428 monitored a photodiode (Photodiode v2.1, <https://www.cf-hw.org/harp/behavior>) through
429 a HARP microprocessor, to measure the light output of the monitor (Dell Latitude 7480). The
430 red, green and blue channels of the display were sent the same values (i.e. grey scale). **A.**
431 Gamma calibration. The input to the display channels was modulated by a linear ramp
432 (range 0-255). Without calibration the monitor output (arbitrary units) increased
433 exponentially (blue line). The measurement was then used to construct an intermediate
434 look-up table that corrected the values sent to the display. Following calibration, the display
435 intensity is close to linear (red line). Inset at top: schematic of the experimental
436 configuration. **B.** Similar to A, but showing the intensity profile of a drifting sinusoidal
437 grating. Measurements before calibration resemble an exponentiated sinusoid (blue dotted
438 line). Measurements after calibration resemble a regular sinusoid (red dotted line).

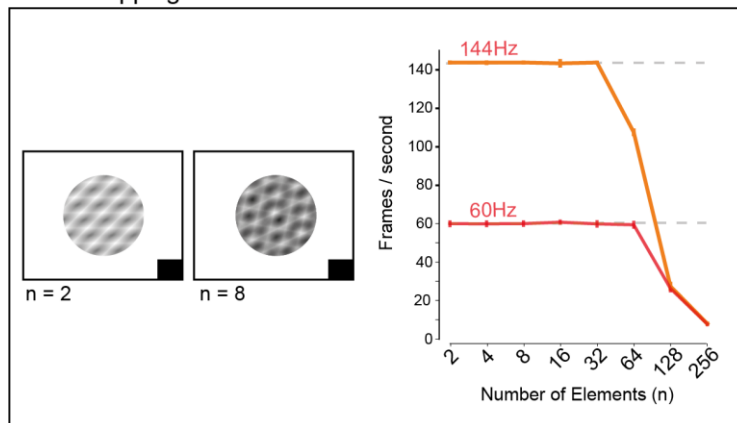
439
440
441 **Figure 3 – video 1: Augmented reality simulation using BonVision.** This video is an example
442 of a deep neural network, trained with DeepLabCut, being used to estimate the position of a
443 mouse’s head in an environment in real-time, and updating a virtual scene presented on the
444 monitors based on this estimated position. The first few seconds of the video display the
445 online tracking of specific features (nose, head, and base of tail) while an animal is moving
446 around (shown as a red dot) in a three-port box (as in Soares, Atallah & Paton, 2016).
447 Subsequently the inset shows the original video of the animal’s movements, which the
448 simulation is based on. The rest of the video image shows how a green field landscape
449 (source: <http://scmapdb.com/wad:skybox-skies>)
450 outside the box would be rendered on three simulated displays within the box (one placed on each of the three oblique walls).
451 These three displays simulate windows onto the world beyond the box. The position of the
452 animal was updated by DeepLabCut at 40 frames/s, and the simulation was rendered at the
453 same rate.

454

A. BonVision Stress test
Non-overlapping textures

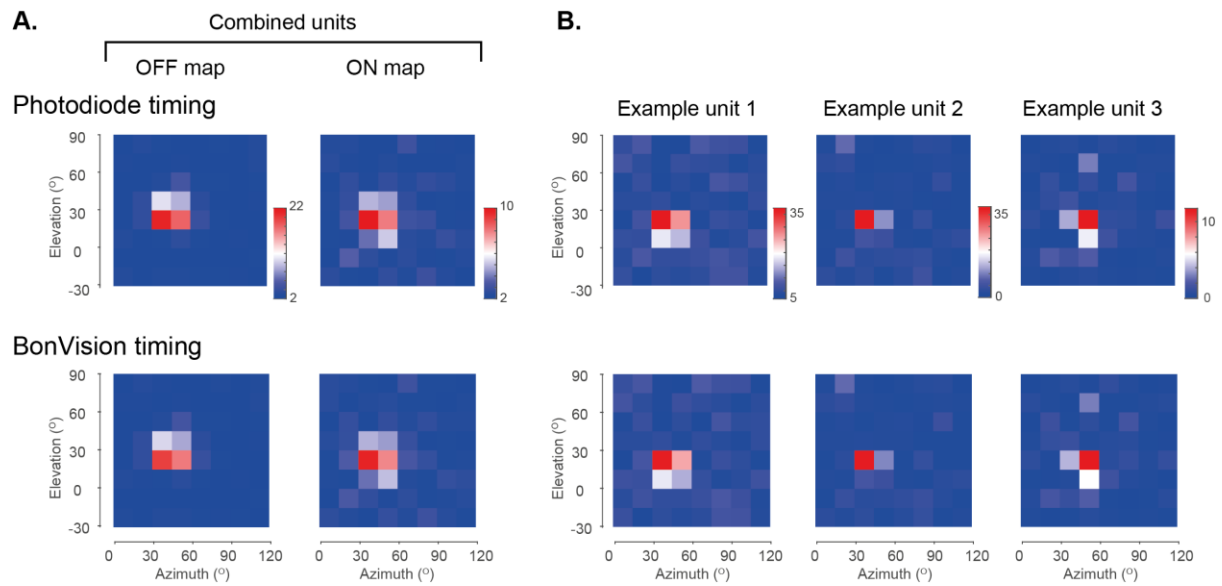


B. Stress tests
Overlapping textures



455
456
457
458
459
460
461
462
463
464
465
466
467
468

Figure 4 - figure supplement 1: BonVision performance benchmarks at high frame rate. A. When using non-overlapping textures BonVision was able to render 576 independent textures without dropping frames at 60Hz. At 144Hz BonVision was able to 256 non-overlapping textures, with no dropped frames, and seldom dropped frames with 576 textures. BonVision was unable to render 1024 or more textures at the requested frame rate. **B.** When using overlapping textures BonVision was able to render 64 independent textures without dropping frames at 60Hz. At 144Hz BonVision was able to render 32 textures, with no dropped frames. Note that these tests were performed on a computer with better hardware specification than that used in Fig 4, which led to improved performance on the benchmarks at 60 Hz. A black square at the bottom right of the screen in A-B is the position of a flickering rectangle, which switches between black and white at every screen refresh. The luminance in this square is detected by a photodiode and used to measure the actual frame flip times.



469

470 **Figure 5 – figure supplement 1: BonVision timing logs are sufficient to support receptive**
 471 **field mapping of spiking activity in superior colliculus of awake mouse.** Top row in each
 472 case shows the receptive field identified using the timing information provided by a
 473 photodiode that monitored a small square on the stimulus display that was obscured from
 474 the animal. Bottom row in each case shows the receptive field identified by using the timing
 475 logged by BonVision during the stimulus presentation (a separate timing system was used to
 476 align the clocks between the computer hosting BonVision and the Open EPhys recording
 477 device). **(A)** Average OFF- and ON receptive field maps for 33 simultaneously recorded units
 478 in a single recording session. **(B)** Individual OFF- receptive field maps for three
 479 representative units in the same session.

480

481 Material and Methods

482

483 Benchmarking

484 We performed benchmarking to measure latencies and skipped (“dropped”) frames. For
485 benchmarks at 60Hz refresh rate, we used a standard laptop with the following
486 configuration: Dell Latitude 7480, Intel Core i7-6600U Processor Base with Integrated HD
487 Graphics 520 (Dual Core, 2.6GHz), 16GB RAM. For higher refresh rates we used a gaming
488 laptop ASUS ROG Zephyrus GX501GI, with an Intel Core i7-8750H (6 cores, 2.20GHz), 16GB
489 RAM, equipped with a NVIDIA GeForce GTX 1080. The gaming laptop built-in display
490 refreshes at 144Hz, and for measuring latencies at 90Hz we connected it to a Vive Pro
491 SteamVR head-mounted display (90Hz refresh rate). All tests were run on Windows 10 Pro
492 64-bit.

493 To measure the time from input detection to display update, as well as dropped frames
494 detection, we used open-source HARP devices from Champalimaud Research Scientific
495 Hardware Platform, using the Bonsai.HARP package. Specifically we used the HARP Behavior
496 device (<https://www.cf-hw.org/harp/behavior>), which is a low latency DAQ, to synchronise
497 all measurements with the extensions: ‘Photodiode v2.1’ to measure the change of the
498 stimulus on the screen, and ‘Mice poke simple v1.2’ as the nose poke device to externally
499 trigger changes. To filter out the infrared noise generated from an internal LED sensor inside
500 the Vive Pro HMD, we positioned an infrared cut-off filter between the internal headset
501 optics and the photodiode. Typically, the minimal latency for any update is 2 frames: one
502 which is needed for the VSync, and one is the delay introduced by the OS. Display
503 hardware can add further delays if they include additional buffering. Benchmarks for video
504 playback were carried out using a trailer from the Durian Open Movie Project (© copyright
505 Blender Foundation | durian.blender.org).

506 All benchmark programs and data are available at

507 <https://github.com/bonvision/benchmarks>.

508 File Formats

509 We tested the display of images and videos using the image and video benchmark
510 workflows. We confirmed the ability to use the following image formats: PNG, JPG, BMP,
511 TIFF, GIF. Movie display relies on the FFmpeg library (<https://ffmpeg.org/>), an industry
512 standard, and we confirmed ability to use the following containers: AVI, MP4, OGG, OGV
513 and WMV; in conjunction with standard codecs: H264, MPEG4, MPEG2, DIVX. Importing 3D
514 models and complex scenes relies on the Open Asset Importer Library (Assimp |
515 <http://assimp.org/>). We confirmed the ability to import and render 3D models and scenes
516 from the following formats: OBJ, Blender.

517 Animal Experiments

518 All experiments were performed in accordance with the Animals (Scientific Procedures) Act
519 1986 (United Kingdom) and Home Office (United Kingdom) approved project and personal
520 licenses. The experiments were approved by the University College London Animal Welfare

521 Ethical Review Board under Project License 70/8637. The mice (C57BL6 wild-type) were
522 group-housed with a maximum of five to a cage, under a 12-hour light/dark cycle. All
523 behavioural and electrophysiological recordings were carried out during the dark phase of
524 the cycle.

525 *Innate Defensive Behaviour*

526 Mice (5 male, C57BL6, 8 weeks old) were placed in a 40cm square arena. A dark refuge
527 placed outside the arena could be accessed through a 10cm door in one wall. A DLP
528 projector (Optoma GT760) illuminated a screen 35cm above the arena with a grey
529 background (80 candela/m²). When the mouse was near the centre of the arena, a 2.5cm
530 black dot appeared on one side of the projection screen and translated smoothly to the
531 opposite side over 3.3s. 10 trials were conducted over 5 days and the animal was allowed to
532 explore the environment for 5-10 minutes before the onset of each trial.

533 Mouse movements were recorded with a near infrared camera (Blackfly S, BFS-U3-13Y3M-C,
534 sampling rate: 60Hz) positioned over the arena. An infrared LED was used to align video and
535 stimulus. Freezing was defined as a drop in the animal speed below 2cm/s that lasted more
536 than 0.1s; flight responses as an increase in the animal running speed above 40cm/s.
537 Responses were only considered if they occurred within 3.5s from stimulus onset.

538 *Surgery*

539 Mice were implanted with a custom-built stainless-steel metal plate on the skull under
540 isoflurane anaesthesia. A ~1mm craniotomy was performed either over the primary visual
541 cortex (2mm lateral and 0.5mm anterior from lambda) or superior colliculus (0.5mm lateral
542 and 0.2mm anterior from lambda). Mice were allowed to recover for 4-24 hours before the
543 first recording session.

544 We used a virtual reality apparatus similar to those used in previous studies (Schmidt-Hieber
545 & Hausser, 2013; Muzzu, Mitolo, Gava & Schultz, 2018). Briefly, mice were head-fixed above
546 a polystyrene wheel with a radius of 10cm. Mice were positioned in the geometric centre of
547 a truncated spherical screen onto which we projected the visual stimulus. The visual
548 stimulus was centred at +60° azimuth and +30° elevation and had a span of 120° azimuth
549 and 120° elevation.

550 *Virtual reality behaviour*

551 5 male, 8-week old, C57BL6 mice were used for this experiment. One week after the
552 surgery, mice were placed on a treadmill and habituated to the Virtual Reality (VR)
553 environment by progressively increasing the number of time spent head fixed: from ~15
554 mins to 2 hours. Mice spontaneously ran on the treadmill, moving through the VR in
555 absence of reward. The VR environment was a 100cm long platform with a patterned
556 texture that animals ran over for multiple trials. Each trial started with an animal at the start
557 of the platform and ended when it reached the end, or if 60s had elapsed. At the end of a
558 trial, there was a 2 second grey interval before the start of the next trial.

559 *Neural Recordings*

560 To record neural activity, we used multi-electrode array probes with two shanks and 32
561 channels (ASSY-37 E-1, Cambridge Neurotech Ltd., Cambridge, UK). Electrophysiology data
562 was acquired with an Open Ephys acquisition board connected to a different computer from
563 that used to generate the visual stimulus.

564 The electrophysiological data from each session was processed using Kilosort 1 (Pachitariu,
565 Steinmetz, Kadir, Carandini & Harris, 2016). We synchronised spike times with behavioural
566 data by aligning the signal of a photodiode that detected the visual stimuli transitions
567 (PDA25K2, Thorlabs, Inc., USA). We sampled the firing rate at 60Hz, and then smoothed it
568 with a 300ms Gaussian filter. We calculated receptive fields as the average firing rate or
569 local field potential elicited by the appearance of a stimulus in each location (custom
570 routines in MATLAB).

571 *Augmented reality for mice*

572 The mouse behaviour videos were acquired by Bruno Cruz from the lab of Joe Paton at the
573 Champalimaud Centre for the Unknown, using methods similar to Soares, Atallah & Paton,
574 2016. A *ResNet-50* network was trained using DeepLabCut (Mathis et al, 2018). We
575 simulated a visual environment in which a virtual scene was presented beyond the arena,
576 and updated the scenes on three walls of the arena that simulated how the view of these
577 objects changed as the animal moved through the environment. The position of the animal
578 was updated from the video file at a rate of 40 frames/s on a gaming laptop: ASUS ROG
579 Zephyrus GX501GI, with an Intel Core i7-8750H (6 cores, 2.20GHz), 16GB RAM, equipped
580 with a NVIDIA GeForce GTX 1080, using a 512x512 video. The performance can be improved
581 using a lower pixel resolution for video capture, and we were able to achieve up to 80
582 frames/s without noticeable decrease in tracking accuracy using this strategy. Further
583 enhancements can be achieved using a *MobileNet* network. The position inference from the
584 deep neural network and the BonVision visual stimulus rendering were run on the same
585 machine.

586 *Human Psychophysics*

587 All procedures were approved by the Experimental Psychology Ethics Committee at
588 University College London (Ethics Application EP/2019/002). We obtained informed
589 consent, and consent to publish from all participants. 4 male participants were tested for
590 this experiment. The experiments were run on a gaming laptop (described above)
591 connected it to a Vive Pro SteamVR head-mounted display (90Hz refresh rate). BonVision is
592 compatible with different headsets (for example Oculus Rift, HTC Vive). BonVision receives
593 the projection matrix (perspective projection of world display) and the view matrix (position
594 of eye in the world) for each eye from the head set. BonVision uses these matrices to
595 generate two textures, one for the left eye and one for the right eye. Standard onboard
596 computations on the headset provide additional non-linear transformations that account for
597 the relationship between the eye and the display (such as lens distortion effects).

598 *Methods References*

599 Mathis, A., Mamidanna, P., Cury, K.M., Abe, T., Murthy, V.N., Mathis, M.W., & Bethge M

600 DeepLabCut: markerless pose estimation of user-defined body parts with deep learning.
601 *Nat. Neurosci.* **21**, 1281–1289 (2018).

602 Muzzu, T., Mitolo, S., Gava, G. P., & Schultz, S. R.. Encoding of locomotion kinematics in the
603 mouse cerebellum. *PLoS ONE*, *13*(9) (2018).

604 Pachitariu, M., Steinmetz, N., Kadir, S., Carandini, M., & Harris, K. *Fast and accurate spike*
605 *sorting of high-channel count probes with KiloSort*. Advances in Neural Information
606 Processing Systems 29. NIPS Proceedings: Barcelona, Spain (2016)

607 Soares, S., Atallah, B., & Paton, J.. Midbrain dopamine neurons control judgement of time.
608 *Science*, *354*(6317), 1273-1277 (2016).

609 Schmidt-Hieber, C., & Hausser, M.. Cellular mechanisms of spatial navigation in the medial
610 entorhinal cortex. *Nat Neurosci*, *16*(3), 325–331 (2013).

611

612 Appendix

613 *Basic workflow structure*

614 Each BonVision workflow starts by loading the basic Shaders library (this is BonVision's
615 implementation of OpenGL) and then creating a window in which stimuli are to be
616 displayed. Bonsai is an event-based framework, so the visual stimulus generation and
617 control are driven by events from the *RenderFrame* or *UpdateFrame* nodes, which are in
618 turn activated when a screen refresh occurs. An event broadcast from the *RenderFrame* or
619 *UpdateFrame* node then activates the cascade of nodes that load, generate or update the
620 different visual stimuli.

621 *Closed-loop control*

622 Parameters of stimuli can also be updated, asynchronously and in parallel, by other events.
623 Parameters of any Bonsai node can be controlled by addressing the relevant property within
624 that node – all parameters within a node can be made visible to the external caller of that
625 node. This is particularly useful for generating closed loop stimuli where the value of these
626 parameters can be linked to external IO devices (for example, position sensors) that are
627 easily accessible using established Bonsai drivers and packages. A major advantage of the
628 Bonsai framework is that the visual stimulus generation does not need to pause to poll
629 those I/O devices, and the values from those devices can be retrieved any time up to the
630 rendering of the frame, creating opportunities for low-lag updating of the visual stimulus.

631 Considerations while using BonVision

632 *Client control*

633 Some experimental designs may rely on complex experimental control protocols that are
634 already established in other software, or are challenging to implement in a reactive
635 framework. For such applications, BonVision's rendering platform can be used as a client to
636 create and control calibrated visual stimuli. This can be implemented using Bonsai's inbuilt
637 IP communication protocols to interact with the independent controller software (for
638 example, Python or MATLAB). BonVision workflows can also be executed from the
639 command-line using standard syntax, without opening the graphical interface of Bonsai.

640 *Mercator projection*

641 A key motivation in developing BonVision was the ability to present 2D and 3D stimuli in the
642 same framework. To enable this, we chose to project 2D stimuli onto a 3D sphere, using the
643 Mercator projection. The Mercator projection, however, contracts longitude coordinates
644 around the two poles, and the consequence is that 2D stimuli presented close to the poles
645 are deformed without compensation. Experiments that require 2D-defined stimuli to be
646 presented near the default poles therefore need particular care. There are a few options to
647 overcome this limitation. One option is to rotate the sphere mapping so that the poles are
648 shifted away from the desired stimulus location. A second option is to present the texture
649 on a 3D object facing the observer. For example, to present a grating in a circular aperture,
650 we could have the grating texture rendered on a disk presented in 3D, and the disk is placed
651 in the appropriate position. Finally, the user can present stimuli via the *NormalisedView*

652 node, which defines stimuli in screen pixel coordinates, using manual calibrations and
653 precomputations to ensure the stimuli are of the correct dimensions.

654 *Constructing 3D environments*

655 There are many well-established software packages with excellent graphical interfaces that
656 are capable of creating 3D objects and scenes, and users are likely to have their preferred
657 method. BonVision therefore focuses on providing easy importing of a wide variety of 3D
658 model formats. BonVision offers three options for building 3D environments:

659 1. BonVision (limited capability). Inbuilt BonVision processes allow for the rendering of
660 textures onto simple planar surfaces. The user defines the position and orientation of each
661 plane in 3D space, and the texture that is to be drawn onto that plane, using the
662 *DrawTexturedModel* node.

663 2. Import (load) 3D models of objects (including cubes, spheres, and more complex models).
664 Common 3D models (such as those used in Fig 1) are often freely available online. Custom
665 models can be generated using standard 3D software, including Blender and CAD programs.
666 The user defines the position of each object, and its dynamics, within BonVision, and can
667 independently attach the desired texture(s) to each of the different faces of those objects
668 using the *DrawTexturedModel* Node.

669 3. Import a full 3D scene (with multiple objects and camera views). BonVision is able to
670 interact with both individual objects and cameras defined within a 3D scene. A particular
671 advantage of this method is that specialised software (e.g. Blender) provide convenient
672 methods to construct and visualise scenes in advance; BonVision provides the calibrated
673 display environment and capacity for interaction with the objects.

674 Once the 3D scene is created, the user can then control a camera in the resultant virtual
675 world that can move and rotate, with BonVision computing the effects of this movement
676 (i.e. without any additional user code) to render what the camera should see onto a display
677 device.

678 *Animation lags and timing logs*

679 While BonVision expends substantial effort to eliminate interruptions to the presentation of
680 a visual stimulus, these can occur, and solutions may be beyond the control of the
681 experimenter. To avoid the potential accumulation of timing errors, the *UpdateFrame* node
682 uses the current time to specify the current location in an animation sequence. The actual
683 presentation time of each frame in an animation can be logged using the standard logging
684 protocols in BonVision. The log can also include the user predefined or real-time updated
685 parameters that were used to generate the corresponding stimulus frame.

686

687 *Customised nodes and new stimuli*

688 Bonsai's modular nature and simple integration with C# and Python scripting means
689 BonVision can be extended by users. The BonVision package is almost entirely implemented
690 using the Bonsai visual programming language, showcasing its power as a domain-specific
691 language. Custom BonVision nodes can be easily created in the graphical framework, or
692 using C# or Python scripting with user-defined inputs, outputs, properties and operations
693 can be generated by users to create novel visual stimuli, define interactions between
694 objects, and enable visual environments which are arbitrarily responsive to experimental
695 subjects.

696 *Physics engine*

697 BonVision is able to calculate interactions between objects using the package
698 Bonsai.Physics, including collisions, bouncing off surfaces or deformations.

699 *Spatial calibration*

700 BonVision provides automatic calibration protocols to define the position of display(s)
701 relative to the observer. A single positional marker is sufficient for each flat display
702 (illustrated in Fig 2; a standard operating procedure is described on the website). An
703 additional marker is placed in the position of the observer, to provide the reference point.

704 When the observer's position relative to the display varies (for example, in the augmented
705 reality example in Fig 3 and Supplementary Video 1), the easiest solution is to calibrate the
706 position of the displays relative to a fixed point in the arena. The observer position is then
707 calculated in real-time, and the vector from the observer to the reference point is added to
708 that from the reference to the display. The resultant vector is the calibrated position of the
709 display relative to the observer's current position.

710 In the case of head-mounted displays (HMDs), BonVision takes advantage of the fact that
711 HMD drivers can provide the calibrated transform matrices from the observer's eye centre,
712 using the *HMDView* node.

713 When the presentation surface is curved (for example, projection onto a dome) a manual
714 calibration step is required as in other frameworks. This calibration step is often referred to
715 as mesh-mapping and involves the calculation of a transformation matrix that specifies the
716 relationship between a (virtual) flat display and position on the projection surface. A
717 standard operating procedure for calculating this mesh-map is described on the BonVision
718 website.

719 *Performance optimisation*

720 We recommend displaying stimuli through a single graphics card, even when multiple
721 displays are used, that is, multiple displays appear to the OS as an extended single display.

722 *Learning to use BonVision*

723 We provide the following learning materials (which will continue to be updated):

724 *Tutorials & Documentation:* <https://bonvision.github.io>

725 *Video tutorials:* <https://www.youtube.com/channel/UCeg-3mfbvjIwbzDVvqYudAA>

726 *Demos & Examples:* <https://github.com/bonvision/examples>

727 *Community forum:* <https://groups.google.com/forum/#!forum/bonsai-users>